

# **Mycoprotein as novel functional ingredient: Mapping of functionality, composition and structure throughout the Quorn fermentation process**

**Lonchamp, J, Stewart, K, Munialo, CD, Evans, L, Akintoye, M, Gordon, S, Clegg, PS, Willoughby, N & Euston, SR**

Published PDF deposited in Coventry University's Repository

Original citation:

Lonchamp, J, Stewart, K, Munialo, CD, Evans, L, Akintoye, M, Gordon, S, Clegg, PS, Willoughby, N & Euston, SR 2022, 'Mycoprotein as novel functional ingredient: Mapping of functionality, composition and structure throughout the Quorn fermentation process', *Food Chemistry*, vol. 396, 133736

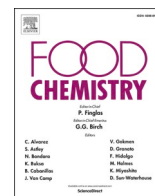
<https://dx.doi.org/10.1016/j.foodchem.2022.133736>

DOI 10.1016/j.foodchem.2022.133736

ISSN 0308-8146

Publisher: Elsevier

This is an Open Access article distributed under the terms of the Creative Commons Attribution License (<http://creativecommons.org/licenses/by/4.0/>), which permits unrestricted use, distribution, and reproduction in any medium, provided the original work is properly cited..



# Mycoprotein as novel functional ingredient: Mapping of functionality, composition and structure throughout the Quorn fermentation process

Julien Lonchamp<sup>a,\*</sup>, Kelly Stewart<sup>b</sup>, Claire D. Munialo<sup>c,1</sup>, Laurence Evans<sup>c</sup>, Muyiwa Akintoye<sup>d</sup>, Susan Gordon<sup>d</sup>, Paul S. Clegg<sup>e</sup>, Nik Willoughby<sup>b</sup>, Stephen R. Euston<sup>b</sup>

<sup>a</sup> School of Health Sciences, Queen Margaret University, Queen Margaret University Drive, Edinburgh EH21 6UU, United Kingdom

<sup>b</sup> Institute of Biological Chemistry, Biophysics and Bioengineering, Heriot-Watt University, Edinburgh EH14 4AS, United Kingdom

<sup>c</sup> Institute of Mechanical, Process & Energy Engineering, School of Engineering and Physical Sciences, Heriot-Watt University, Edinburgh EH14 4AS, United Kingdom

<sup>d</sup> Quorn Foods, Station Road, Stokesley TS9 7BR, United Kingdom

<sup>e</sup> School of Physics & Astronomy, The University of Edinburgh, Peter Guthrie Tait Road, Edinburgh EH9 3FD, United Kingdom

## ARTICLE INFO

### Keywords:

Quorn  
Mycoprotein  
Functionality  
Composition  
Structure

## ABSTRACT

This study provides the first mapping of mycoprotein functionality, composition and structure throughout the Quorn fermentation process. The fermentation broth, RNA-reduced broth (RNA-broth), centrate and their centrifugation deposits and supernatants were characterised. The broth, RNA-broth and their deposits displayed high concentrations of fungal filaments, which contributed to their high gelling properties (with a 5,320 Pa elastic modulus reported for RNA-broth deposits gels). Foams prepared with RNA-broth and centrate supernatants via frothing exhibited high stability (380 min), with high concentrations of a foam-positive cerato-platanin reported in these samples. Emulsions prepared with the broth and broth supernatant showed high emulsifying activity and stability indexes (12.80 m<sup>2</sup>/g and 15.84 mins for the broth supernatant) and low oil droplet sizes (18.09 μm for the broth). This study identified previously unreported gelling, foaming and/or emulsifying properties for the different Quorn streams, highlighting opportunities to develop novel sustainable alternatives to animal-derived functional ingredients using mycoprotein material.

## 1. Introduction

In order to reduce the environmental impact of the food industry, sustainable alternatives to animal-derived functional ingredients such as milk and egg proteins, which are commonly used as gelling, foaming or emulsifying agents, need to be developed (McMichael, Powles, & Butler, 2007). The production of biomass by fermentation is a potential source of such sustainable alternatives. Mycoprotein refers to the protein-rich biomass produced by Quorn Foods using the *Fusarium venenatum* A3/5 fungus for use in their meat alternative formulations. This process has been shown to generate significantly lower greenhouse gas emissions and land and water footprints than meat-based processes (Finnigan, Lemon, Allen, & Patton, 2010).

The mycoprotein production process comprises several stages. Following fermentation in air-lift fermenters, the broth (concentrated in

fungal filaments or hyphae) is first heat-shocked above 68 °C for 30 to 45 min. This heating step stops fungal growth and disrupts ribosomes, resulting in the activation of RNases which denature RNA into nucleotides (Ward, 1996). This RNA-reduction step is necessary to ensure the nucleic acid content is at a safe level for consumption below 2 % w/w as recommended by the WHO (Ward, 1996). The resulting RNA-reduced broth undergoes a second heating step at 90 °C, which inactivates the fungus via alteration of its cellular structures and functions, and subsequent centrifugation. The centrifugation deposit is the mycoprotein biomass, which is further processed into meat alternative products, while the liquid supernatant is referred to as centrate. The RNA-reducing heat-shock treatment damages the fungal cell wall, which leads to the diffusion of a fraction of the cell components (Ward, 1996). As a result the centrate contains hyphal material, proteins and metabolites in addition to fermentation feedstock residues. Despite being currently an

**Abbreviations:** WPC, whey protein concentrate; mRNA, messenger RNA; NCM, nitrogen-containing material; EAI, emulsifying activity index; ESI, emulsion stability index.

\* Corresponding author.

E-mail address: [JLonchamp@qmu.ac.uk](mailto:JLonchamp@qmu.ac.uk) (J. Lonchamp).

<sup>1</sup> Present address: School of Life Sciences, Coventry University, Priory Street, Coventry, CV1 5FB, UK.

<https://doi.org/10.1016/j.foodchem.2022.133736>

Received 17 August 2021; Received in revised form 8 July 2022; Accepted 15 July 2022

Available online 20 July 2022

0308-8146/© 2022 The Author(s). Published by Elsevier Ltd. This is an open access article under the CC BY license (<http://creativecommons.org/licenses/by/4.0/>).

unexploited co-product stream, the centrate foams in the centrifuge, which suggests that surface-active material is present among these components.

We previously reported that a centrate extract obtained via 100 kDa ultrafiltration (R100 or retentate 100) displayed high functional properties (Lonchamp, Clegg, & Euston, 2019). R100 solutions exhibited high viscosity, whilst R100 hydrogels displayed high viscoelasticity. R100 foams proved very stable, whilst oil-in-water R100 emulsions displayed small and stable oil droplets. R100 solutions and gels showed large hyphal aggregates, which contributed to their high viscosity and viscoelasticity. R100 foams were also characterised by a dense hyphal network, which contributed to their stability. In addition, the presence of interfacially-active molecules in R100 was demonstrated via interfacial tension measurements, in which a rigid film was observed at the oil/water interface and stabilised the oil droplets. Metabolomic and proteomic analyses of the centrate showed the presence of a range of functional metabolites and proteins, including a cerato-platanin protein, cell wall components (including chitin and chitosan), guanine and guanine-based nucleosides and nucleotides.

A number of surface-active protein families of filamentous fungal origin have been reported, including cerato-platanins (Frischmann et al., 2013). The cerato-platanin EPL1 from *Trichoderma atroviride* was shown to self-assemble into films at air/water interfaces, leading to strong foaming properties (Frischmann et al., 2013). In addition, cerato-platanins isolated from the marine fungi *Aspergillus terreus* MUT 271 and *Trichoderma harzianum* MUT 290 displayed high surface-active properties, whilst emulsions prepared with these isolates showed high stability (Pitocchi et al., 2020).

Mycoprotein also contains a number of carbohydrates with known functional properties, including the fungal cell wall components *N*-acetylglucosamine polymers chitin and chitosan (Denny, Aisbitt, & Lunn, 2008). Chitin, chitosan and their derivatives display high emulsifying, thickening and gelling properties (Lapasin, Stefancic, & Delben, 1996), including those of fungal origin (Quintela, Villarán, López De Armentia, & Elejalde, 2012). Finally, high levels of nucleotides are present in the centrate following the breakdown of RNA during the heat-shock RNA-reduction step (Ward, 1996). Guanine-based nucleotides display high thickening and gelling properties due to the ability of guanine to self-associate (Peters & Davis, 2016).

We also previously studied the impact of sonication on the functionality and structure of the R100 extract (Lonchamp, Akintoye, Clegg, & Euston, 2020). The characteristic large hyphal structures of this extract were broken down into smaller fragments following ultrasonic treatment. The sonicated R100 solution was then used to prepare oil-in-water emulsions, which oil droplet sizes proved smaller than emulsions prepared with untreated R100. Confocal micrographs showed a ring of small hyphal fragments around oil droplets in both untreated and sonicated R100 emulsions. These results suggested that small hyphal fragments present in R100 and/or released during processing (sonication and/or emulsification) contributed to forming and stabilising small oil droplets via a Pickering-type mechanism. This material is compatible with the shape and size requirements of Pickering stabilisation for foam and emulsion systems (Lam, Velikov, & Velev, 2014). *Lycopodium clavatum* moss spores were shown to stabilise oil-in-water emulsions (Binks, Clint, Mackenzie, Simcock, & Whitby, 2005), whilst Dorobantu, Yeung, Foght, and Gray (2004) reported the ability of bacterial cells to produce stable water-in-oil and oil-in-water emulsions.

Overall, our previous studies (Lonchamp et al., 2020; Lonchamp et al., 2019) showed the potential of an extract from the Quorn fermentation co-product (centrate) as novel functional ingredient and the complex nature of mycoprotein functionality due to the presence of a range of functional components including hyphal structures and interfacially-active molecules. However, to date the functionality of the mycoprotein material has not been systematically assessed throughout the Quorn fermentation process and the functional profile of the two main streams (fermentation broth and RNA-reduced broth) has not been

fully characterised. In addition the relationship between the functionality of the mycoprotein material and its structure and composition has not been systematically studied. In particular the impact of the two heating steps of the Quorn process on mycoprotein composition, structure and functionality has not been determined. This current study addresses this gap of knowledge by assessing and comparing the functionality of the different Quorn fermentation streams (fermentation broth, RNA-reduced broth and centrate) while characterising their compositions and structure. The aim of this work is to assess the potential to develop novel sustainable alternatives to animal-derived functional ingredients using mycoprotein material from one or several Quorn fermentation streams. We hypothesised that the functionality of the broth and RNA-reduced broth (whole streams and centrifugation deposits) was mainly governed by hyphal material while the functionality of the different stream supernatants was mainly governed by surface-active compounds, and that mycoprotein functionality was modified by the two heating steps of the process.

## 2. Material and methods

### 2.1. Sample collection

The fermentation broth (named broth), RNA-reduced broth (named RNA-broth) and centrate streams were collected from the Quorn fermenter site at Billingham (UK) at the mid-point of the fermentation cycle (day 19). A preliminary study showed that the functional properties of the different streams were both high and consistent at the mid-fermentation point in comparison with other stages of the cycle (results not shown). The RNA-broth was collected following the first heating step, which was a 68 °C heat-shock RNA reduction of the fermented broth as described by Ward (1996). The centrate was collected following the second heating step (90 °C) and centrifugation of the RNA-reduced broth, as described by Ward (1996). The samples were frozen at -20 °C and sent to QMU.

### 2.2. Sample processing

The samples were thawed in a cold room set at 4 °C before analysis. The different streams were then centrifuged at 10,000 × g at 4 °C for 30 min using an AVANTI J-265 centrifuge (Beckman Coulter, UK). Samples of the whole streams, centrifugation deposits (named deposits) and centrifugation supernatants (named supernatants) were freeze-dried using a Super Modulyo unit (Edwards, UK). The purpose of comparing the RNA-broth supernatant (which underwent the first heating step) and the centrate (which is the equivalent of the RNA-broth supernatant after the second heating step) was to assess the impact of the second heating step (90 °C) on the composition and functionality of the material.

### 2.3. Methodology

The functional profile (rheological, foaming and emulsifying properties) of the different Quorn fermentation streams (fermentation broth, RNA-reduced broth and centrate) and of their soluble and insoluble fractions (centrifugation supernatants and deposits) was assessed while their composition was determined by metabolomic and proteomic analyses and their structure was characterised via microscopy. Lacprodan 87, a commercial whey protein concentrate (WPC) manufactured by Arla (Denmark), was chosen as control for the rheological, foaming and emulsifying tests to assess the potential of the samples as functional ingredients for the food industry.

### 2.4. Nitrogen content

Our previous study highlighted that centrate contained a large range of nitrogen-containing molecules including constituents of fungal cell membranes and cell walls (including proteins, chitin, chitosan, phos-

pholipids, glycosphingolipids and sphingomyelins) (Lonchamp et al., 2019). In order to standardise sample quantities to be used for the functional tests, the AOAC Kjeldahl method (Lynch, Barbano, & Fleming, 1998) was used to measure the nitrogen-containing material (NCM) content of the samples. Sets of 0.1 g of the samples (whole stream, centrifugation deposit and centrifugation supernatant of each of the broth, RNA-broth and centrate) were digested in concentrated sulphuric acid (92 %) at 440 °C in the presence of a selenium catalyst using a Kjeltex Basic Digestion Unit 20 (Foss, UK). The samples were then distilled into boric acid using a Tecator Kjeltex 8100 Manual Distillation Unit (Foss, UK). The distilled samples were finally titrated using 0.1 mol/L hydrochloric acid. The % nitrogen was calculated using the following formula:

$$\% \text{ Nitrogen} = \frac{\text{Titration volume (ml)} \times 14.007}{\text{Sample weight (g)} \times 100}$$

The general conversion factor used by Quorn Foods (6.25) was used to obtain the % nitrogen-containing material NCM (replacing the term % crude protein given the high concentrations of non-protein nitrogen-containing molecules). The experiment was repeated thrice, and three replicates of each sample were analysed for each experiment.

## 2.5. Gel electrophoresis

Sodium dodecyl sulfate polyacrylamide gel electrophoresis (SDS-PAGE) was performed on the nine samples using a Mini-Protean Tetra Cell System with TGX 4–20 % Tris-glycine gels (Bio-Rad Laboratories Ltd., UK). The method described by Havea, Watkinson, and Kuhn-Sherlock (2009) was followed with minor modifications (Lonchamp et al., 2019). Solutions (1 % w/w NCM) of the samples were prepared in deionised water, stirred for one hour and mixed at a 1:1 ratio with Laemmli 2x concentrate sample buffer (Sigma Aldrich Ltd., UK). The mixtures were heated at 70 °C for 10 min. In parallel native PAGE samples were prepared by mixing the solutions with Novex native TrisGly 2x sample buffer (Life Technologies, UK) at a 1:1 ratio. The See Blue Plus2 pre-stained protein ladder standard (Thermo Fischer, UK) was chosen as molecular weight marker. 20 µl of sample or 10 µl of marker were loaded onto the wells, following which the gels were run for 1 h at 100 V in Tris/Glycine/SDS buffer (Bio-Rad Laboratories Ltd., UK). The gels were subsequently stained in a Coomassie brilliant blue solution (VWR Ltd., UK) and destained in glacial acetic acid:methanol:deionised water at a 1:4:5 ratio. The gels were scanned using a ChemiDoc XRS + imaging system (Bio-Rad Laboratories Ltd., UK) and the analysis was carried out using the associated Image Lab software.

## 2.6. Proteomics

Four samples were analysed: broth, RNA-broth, RNA-broth supernatant and centrate. The RNA-broth supernatant (centrifugation supernatant of the RNA-broth) was included in this analysis to assess the impact of the second heating step on the composition of the centrate (which is the equivalent to the RNA-broth supernatant after this second heating step). The method developed by Le Bihan et al. (2011) was used for protein digestion. The samples were denatured in 8 M urea then reduced by incubation with dithiothreitol. The samples then underwent cysteine alkylation with iodoacetamide and were subsequently digested overnight using 60 µg trypsin. Four µg of each sample were then acidified with 1 % formic acid, following which the samples were centrifuged and vacuum-dried. The extracts were analysed by capillary HPLC-MSMS following a method developed by Martin, Munagapati, Salvo-Chirnside, Kerr, and Le Bihan (2012) on a hybrid LTQ-Orbitrap XL instrument (Thermo-Fisher, UK) using 140-minute gradients, HPLC-quality acetonitrile (Fisher, UK), suprapure formic acid and sequencing-grade trifluoroacetic acid (Merck, Germany). Multicharged (2+, 3+ and 4+) ion intensities were extracted from the LC-MS files. The MSMS data were then compared against the NCBI protein database

using the Mascot Version 2.4 software (Matrix Science Ltd, UK) with a maximum missed-cut value of 2, variable oxidation, N-terminal protein acetylation, fixed carbamidomethylation, precursor mass tolerance of 7 ppm and MSMS tolerance of 0.4 Da. A significance threshold of <0.05 was chosen and the minimum peptide cut-off score was set at 20. The criteria for protein retention were their identification using the *Fusarium* proteome and quantification with 2 or more peptide sequences. Six replicates were analysed per sample.

## 2.7. Metabolomics

Similarly to the proteomic analysis, the broth, RNA-broth, RNA-broth supernatant and centrate were also analysed for metabolomic composition. Alcohol-insoluble residues of the samples were produced in 10 ml of 70 % ethanol. The vials were left overnight at room temperature, and were then washed thrice with 10 ml of a 10:10:3 chloroform:methanol:water solution by successive centrifugations at 2,700 × g for 10 min. The resulting supernatants were pooled and run in positive (pos) and negative (neg) ion mode on a 6560 Agilent Quadrupole Time of Flight (IM-QTOF) mass spectrometer (MS) (Agilent, UK) equipped with a 100 mm × 2.1 mm, 1.8 µm ACE C18-PFP column. The apparatus was run in both ion mobility QTOF mode and MSMS QTOF mode. The following gradient elution was programmed using the two solvents A (50 % methanol) and B (95 % acetonitrile): 0 min (10 % B), 5 min (30 % B), 10–12 min (95 % B), 15–16 min (10 % B). The flow rate was set at 0.2 ml/min. Data analysis was carried out using Mass Profiler (MP) and data extraction was undertaken via Profinder. Cluster analysis was then performed using Mass Profiler Professional (MPP). The samples were aligned with the Metlin accurate mass metabolite database using accurate mass matching of 10 ppm. Six replicates were analysed per sample.

## 2.8. Rheological properties

The viscosity and gelation profiles of the samples were measured using a Bohlin Gemini controlled stress rheometer (Malvern Instruments, UK) equipped with cone-and-plate geometry. Solutions (10 % w/w NCM) of the broth, broth deposit, RNA-broth and RNA-broth deposit were prepared in deionised water and stirred for two hours. The WPC rheological control was prepared at the same solid content (18 % w/w) as the 10 % w/w NCM broth solution to rule out the potential impact of solid content on the viscosity of the samples.

Viscosity measurements were performed at 20 °C using a 4°/40 mm cone (gap 150 µm). The samples underwent a shear rate increase from 0.001 s<sup>-1</sup> to 50 s<sup>-1</sup> with measurement of instantaneous viscosity (Pa.s). The shear viscosity data obtained as a function of shear rate were fitted to the following power-law model:

$$\eta = K\dot{\gamma}^{n-1}$$

where  $\eta$  = viscosity (Pa.s),  $K$  = consistency coefficient (Pa.s<sup>n</sup>),  $\dot{\gamma}$  = shear rate (s<sup>-1</sup>) and  $n$  = power law coefficient. The model was linearised by converting the data to their logarithmic values:

$$\log(\eta) = \log(K) + (n - 1)\log(\dot{\gamma})$$

Log( $\eta$ ) was plotted as a function of log( $\dot{\gamma}$ ) for each sample and the  $K$  value was determined at the 1 s<sup>-1</sup> shear rate value.

Prior to the gelation tests, the linear viscoelastic region of the samples was determined by measuring the elastic modulus ( $G'$ ) and viscous modulus ( $G''$ ) in oscillation mode at 1 Hz over a strain amplitude sweep of 0.00005 to 50. Gelation profiles were then assessed via small-amplitude oscillatory measurements using a 2°/40 mm cone (gap 70 µm), 1 Hz frequency and a strain value chosen within the linear viscoelastic region of each sample. The samples underwent a temperature sweep from 40 to 90 °C in up-down mode (15-minute up-sweep, 15-minute down-sweep) with  $G'$  and  $G''$  measured. The experiments were repeated thrice, with three replicates analysed per sample for each

experiment.

## 2.9. Foaming properties

Fifteen g solutions (1 % w/w NCM) of the nine samples and the WPC control were prepared in 50 ml glass beakers, which corresponds to an initial volume of 18 cm<sup>3</sup> (1.4 cm sample height and 4 cm beaker diameter), and stirred for one hour. The solutions were frothed for 1 min using a handheld whisk-type frother (Aerolatte, UK). The initial height of the foam was measured, followed by measurements every 10 min until the foam collapsed. The foaming ability was determined by the initial foam height, whilst the time needed for the foam to collapse indicated its stability. The experiment was repeated four times, with three replicates of each sample analysed for each experiment.

## 2.10. Emulsifying properties

The oil-in-water emulsifying properties of the nine samples and the WPC control were assessed via oil droplet size distribution, emulsifying activity index (EAI) and emulsion stability index (ESI) measurements. A method developed by Ogunwolu, Henshaw, Mock, and Santos (2009) was used with minor modifications (Lonchamp et al., 2019) to determine the EAI and ESI. Each 1 % w/w NCM solution was prepared at a weight of 22.5 g and mixed with 7.5 g of sunflower oil to obtain a 3:1 water:oil phase ratio. The mixtures were homogenised using an IKA T18 Ultra-Turrax high-speed homogeniser (IKA-Werke GmbH, Germany) for 1 min at 10,000 rpm. Fifty µl of each emulsion were collected from the bottom of the vials following emulsification and added to 5 ml of a 0.1 % w/v SDS solution. The absorbance of the resulting solutions was measured at 500 nm using a Genesys 6 UV/Vis spectrophotometer (Thermo Electron Corporation, USA). The same procedure was repeated after 10 min. The emulsifying activity index EAI (which represents the ability of the sample to form an emulsion) and the emulsion stability index ESI were calculated using the following formulae:

$$EAI(m^2/g) = \frac{2 \times T \times A_0 \times \text{dilutionfactor}}{C \times \varnothing \times 1000} \quad ESI(\text{min}) = \frac{A_0}{A_0 - A_{10}} \times \Delta t$$

where T = 2.303, A<sub>0</sub> = apparent absorbance at 0 min, dilution factor = 100, C = weight per unit volume (g/mL), Ø = oil volumetric fraction (0.25), A<sub>10</sub> = apparent absorbance after 10 min, Δt = 10 min. The experiment was repeated thrice, with three replicates of each sample analysed for each experiment.

The average oil droplet size distribution of the emulsions or D[3,2] (surface weighted mean) was measured using a Mastersizer 2000 (Malvern Instruments Ltd., UK) set at the refractive index of sunflower oil (1.474) and at 10 % laser obscuration adjustment. The experiment was repeated thrice, with three replicates per sample analysed for each experiment.

## 2.11. Microscopy of solutions and dried foams

Solutions (1 % w/w NCM) of the nine samples and dried foams prepared with these solutions were imaged using a Zeiss Axioptol brightfield microscope (Zeiss, Germany). The foams were prepared according to the method presented in section 2.7 (Foaming properties). Aliquots of each foam were placed in microscope slides and left to dry for 24 h before imaging to observe the hyphal structures present. A 40x/0.75 lens was used and micrographs were analysed using the associated Zen software.

A sonicated centrate extract we characterised in our previous study (Lonchamp et al., 2020) was also imaged to provide a size reference for fragments obtained following breakdown of large hyphal structures. To produce this sample, a 1 % w/w NCM solution of the retentate R100 fraction (resulting from a 100 kDa ultrafiltration of the centrate) was sonicated using a Sonics Vibra-Cell VCX-500 probe sonicator (Sonics,

UK) for 3 min at 500 Watts, 20 kHz and 50 % amplitude.

## 2.12. Microscopy of emulsions and hydrogels

Hydrogels and oil-in-water emulsions of the nine samples were imaged using a Leica TCS2 confocal laser scanning microscope (Leica Microsystems, Germany). The micrographs were recorded at a 512 × 512 pixel resolution and analysed using the DM SDK software (version 4.2.1). The fluorescent dye Rhodamine B was added to 10 % w/w NCM solutions of the nine samples for the imaging of hydrogels in order to stain the hyphal material. The gels were obtained according to the method presented in section 2.6 (Rheological properties). The dye was excited at 514 nm, the collection range was set at 600–700 nm and a 10x/0.25 dry lens was used. The emulsions were obtained according to the method presented in section 2.8 (Emulsifying properties). The oil was supplemented with traces of Nile Red dye (Sigma Aldrich Co., UK) before mixing with the solutions in order to stain the resulting emulsion droplets. The dye was excited at 549 nm, the emission maximum was set at 628 nm for fluoresced light collection and a 63x/1.40–0.60 oil lens was used.

## 2.13. Statistical analysis

Statistical analysis of the data obtained for the Kjeldahl, viscosity, gelling, frothing and EAI/ESI assays and the proteomic and metabolomic analyses was carried out using the SPSS Statistics 23.0 software (IBM, USA). One-way ANOVA tests were performed, followed by post hoc Tukey's HSD (honestly significant difference) tests for pair-wise multiple comparison. A p value of 0.05 was used as cut-off for significance.

The concentrations of a specific protein or metabolite measured in two different samples were deemed significantly different if a statistical difference was reported (p < 0.05) and if the ratio between the two concentrations was above 2 or below 0.5 (+/- 10 %) in order to minimise the effect of material variability based on previous metabolomic work (Shaw et al., 2016).

## 3. Results and discussion

### 3.1. Characterisation of the different streams

The whole streams and centrifugation deposits of the broth and RNA-broth showed similar nitrogen-containing material (NCM) contents (including protein and non-protein material), from 52.2 % to 57.8 % (p > 0.05). The NCM content of the centrate proved significantly lower than these values (46.4 %) (p < 0.05). The NCM contents of the RNA-broth and centrate supernatants were similar to the centrate value (45.4 %) (p > 0.05) and statistically higher than the broth supernatant (40.8 %) (p < 0.05), which confirmed the diffusion of soluble nitrogen-containing material through the cell wall as a result of the first heating step (68 °C heat-shock RNA reduction of the fermented broth) (Ward, 1996). The centrate deposit showed a significantly higher NCM content than the other samples (82.3 %) (p < 0.05). This 71 % NCM increase in comparison with the RNA-broth deposit suggested the aggregation of nitrogen-containing material during the second heating step (90 °C heating of the RNA-reduced broth).

Due to the complexity of the material, a number of bands on the SDS-PAGE gel appeared blurred or smeared (Fig. 1). Similar issues were previously reported by Colosimo et al. (2020) for a cell-free mycoprotein extract and by Griffen, Wiebe, Robson, and Trinci (1997) for filtered Quorn fermentation broth. The sharpness, brightness and contrast of the scanned gel was optimised in order to present and visualise both concentrated and weak bands from the different streams at the same time (Fig. 1). An additional unprocessed image of two weak bands specific to the RNA-broth and centrate supernatants but not clearly visible on the processed gel image (bands [i] and [j]) is provided in Fig. 1 to highlight their presence.

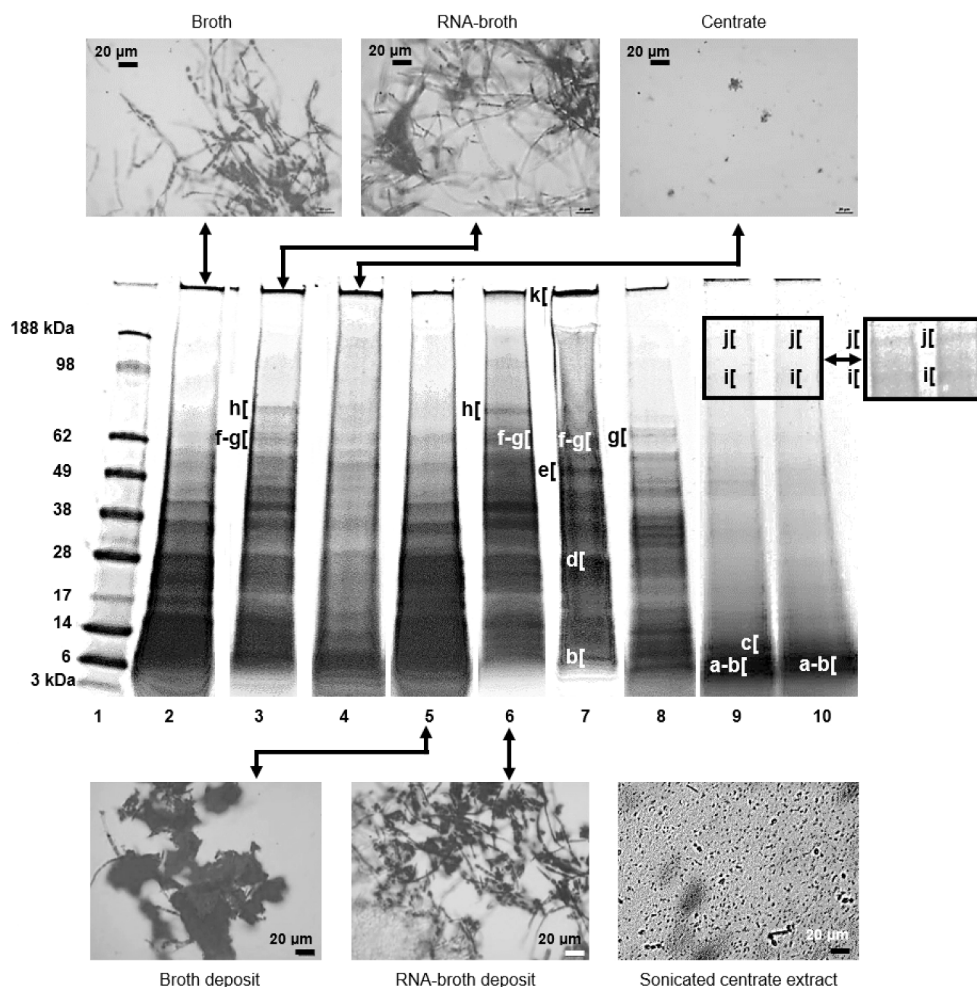


**Fig. 1.** SDS-PAGE profiles of the broth, RNA-broth, centrate and their centrifugation deposits and supernatants with corresponding bright-field micrographs of the solutions and of a sonicated centrate extract solution (1 % w/w NCM solutions, magnification  $\times 50$ ). See Blue reference marker [lane 1], broth [2], RNA-broth [3], centrate [4], broth deposit [5], RNA-broth deposit [6], centrate deposit [7], broth supernatant [8], RNA-broth supernatant [9], centrate supernatant [10].

A fraction of the centrate deposit did not migrate on the SDS-PAGE gel with the presence of the concentrated band [k], indicating the presence of material  $>200$  kDa (which corresponds to the higher size of protein marker band). Faint bands [k] were also reported for the other samples. These results further supported the potential aggregation of nitrogen-containing material during the second heating step, resulting in large aggregates in the centrate deposit. A concentrated low molecular band [b] was reported in the RNA-broth supernatant and the centrate supernatant and deposit, as well as a concentrated band [a] in the RNA-broth and centrate supernatants and a concentrated band [c] in the centrate deposit and RNA-broth supernatant. Faint bands [a], [b] and [c] were observed in the other samples, indicating that the corresponding low-molecular weight proteins could have been released during the two heating steps. Similarly to the results obtained for the RNA-broth and centrate supernatants, Colosimo et al. (2020) reported a band of similar size (circa 5 kDa) to band [a] in a protein extract from the mycoprotein biomass (following the removal of the cell wall material), confirming their presence in supernatant fractions following the two heating steps.

Bands [d] and [e] were specifically concentrated in the centrate deposit in comparison with other samples and could correspond to monomeric or oligomeric forms of protein aggregates formed during the two heating steps and subsequently broken down in presence of SDS and  $\beta$ -mercaptoethanol during sample preparation. A band of similar size to [e] was observed by Colosimo et al. (2020) in the cell-free mycoprotein extract, confirming its presence in the centrate following the two heating

steps.

The RNA-broth, RNA-broth deposit and centrate deposit displayed two concentrated bands [g] and [h] in comparison with the other samples (except the broth supernatant for band [g]), which could correspond to proteins released during the two heating steps. A band [h] was specifically observed in the RNA-broth and its deposit, indicating a possible protein release during the RNA-reducing step. The RNA-broth and centrate supernatants displayed two specific bands [i] and [j], which could correspond to soluble proteins released during the two heating steps. Colosimo et al. (2020) also reported a band in the cell-free mycoprotein extract at a similar molecular weight to band [i], confirming its presence in supernatant fractions following the two heating steps.

A specific band was observed at circa 31 kDa in the broth supernatant, indicating that this protein was affected by the heating processes. Griffen et al. (1997) also reported a band in the filtered Quorn fermentation broth at this molecular weight, confirming its presence in the broth supernatant.

Micrographs of the broth, RNA-broth and their deposits showed a concentration of fungal filaments and a number of filament aggregates (Fig. 1). The formation of fungal aggregates results from combined hydrophobic and electrostatic interactions between cell wall components including proteins or polysaccharides (Zhang & Zhang, 2016).

A number of small spherical components were observed on the centrate micrograph (Fig. 1). A high density of these components was also observed among small cell fragments in the sonicated centrate

extract (Fig. 1). These small spherical components could correspond to stress granules or processing bodies (p-bodies), which would have formed as a result of the stress caused by the heat-shock RNA-reduction process (and the additional sonication for the sonicated centrate extract). These components would then have diffused through the cell walls of damaged cells into the centrate. Stress granules are messenger ribonucleoprotein (mRNP) aggregates composed of proteins and RNA molecules that usually form upon cellular stress, while p-bodies are composed of enzymes involved in messenger RNA (mRNA) turnover. Stress granules were previously shown to form and the number and size of p-bodies to increase as a response to heat stress in the filamentous fungus *Aspergillus oryzae* heated at 45 °C for 10 min (Huang, Maruyama, & Kitamoto, 2013).

### 3.2. Composition of the different streams

Table 1 lists the major proteins present at different concentrations in broth, RNA-broth, RNA-broth supernatant and centrate streams. Two

hundred and ninety-seven proteins were reported according to criteria defined by Pappin, Hojrup, and Bleasby (1993): identification with more than one peptide and MOWSE scores equal to or above 85 (with a 5 % probability of misidentification). Nine stress-induced proteins (including 8 heat-shock proteins) were identified, with six of them present in significantly higher concentrations in the RNA-broth in comparison with the broth following the heat-shock RNA-reduction step ( $p < 0.05$ ).

A cerato-platanin (FGSG\_04471) was identified in all four samples. Our previous study (Lonchamp et al., 2019) reported a higher concentration of this protein in the R100 functional centrate extract in comparison with less functional centrate extracts. In the current work the concentration of this cerato-platanin increased following the RNA-reduction heating step, with statistically higher concentrations in the RNA-broth supernatant and centrate in comparison with the broth and RNA-broth ( $p < 0.05$ ). The cerato-platanin was quantified as the 9th and 8th most abundant protein respectively in the RNA-broth supernatant and centrate. Cerato-platanin proteins (CPPs) have been identified in

**Table 1**

Proteomic comparison of the fermentation broth, RNA-broth, RNA-broth centrifugation supernatant and centrate.

Identification	Reported functions and properties	Molecular mass in kDa (PAGE band)	Centrate/RNA-broth supernatant	Centrate/RNA-broth	Centrate/Broth	RNA-broth supernatant/RNA-broth	RNA-broth supernatant/Broth	RNA-broth/Broth
Heat shock 70 kd protein cognate 1	Stress response	60 (f-g)	2.59 ± 0.31 *	0.42 ± 0.05 *	5.09 ± 0.67 *	0.16 ± 0.03 *	1.97 ± 0.20 *	12.05 ± 1.36 *
30 kDa heat shock protein	Stress response	24 (d)	1.28 ± 0.19	9.38 ± 1.04 *	1.24 ± 0.11	7.33 ± 0.88 *	0.97 ± 0.12	0.13 ± 0.02 *
Heat shock protein 60	Stress response	16 (c)	2.75 ± 0.35 *	0.32 ± 0.04 *	0.64 ± 0.05	0.12 ± 0.02 *	0.23 ± 0.02 *	1.99 ± 0.30 *
Heat shock protein 70	Stress response	71 (h)	1.83 ± 0.30	1.52 ± 0.22	8.32 ± 0.93 *	0.83 ± 0.10	4.55 ± 0.62 *	5.49 ± 0.71 *
Heat shock protein 90	Stress response	79 (i)	2.23 ± 0.19 *	0.83 ± 0.09	3.92 ± 0.46 *	0.37 ± 0.05 *	1.76 ± 0.26	4.72 ± 0.62 *
Heat shock protein SSB1	Stress response	67 (f-g)	1.21 ± 0.18	0.26 ± 0.04 *	0.81 ± 0.09	0.21 ± 0.02 *	0.67 ± 0.08	3.11 ± 0.44 *
Heat shock protein 60	Stress response	68 (f-g)	1.63 ± 0.28	0.69 ± 0.06	0.39 ± 0.05 *	0.43 ± 0.05 *	0.24 ± 0.02 *	0.57 ± 0.07
Heat shock protein 98	Stress response	103 (j)	0.66 ± 0.08	2.23 ± 0.18 *	0.75 ± 0.09	3.40 ± 0.50 *	1.14 ± 0.21	0.34 ± 0.04 *
<b>Total heat-shock proteins</b>			1.84 ± 0.23	1.13 ± 0.17	4.02 ± 0.56 *	0.61 ± 0.08	2.18 ± 0.28 *	3.56 ± 0.51 *
Stress-induced-phosphoprotein 1	Stress response	65 (f-g)	1.44 ± 0.24	6.24 ± 0.89 *	12.17 ± 1.76 *	4.32 ± 0.51 *	8.42 ± 0.99 *	1.95 ± 0.24 *
PBP1 (Pab1p interacting protein)(LsmAD domain-containing protein)	RNA decapping	100 (j)	2.06 ± 0.31 *	37.88 ± 5.04 *	169.59 ± 20.49 *	18.39 ± 2.53 *	82.31 ± 10.02 *	4.48 ± 0.60 *
Pab (Polyadenylate-binding protein)	RNA decapping	81 (i)	0.52 ± 0.04 *	1.54 ± 0.22	8.05 ± 0.77 *	2.98 ± 0.48 *	15.52 ± 1.93 *	5.21 ± 0.76 *
Lsm14 (Lsm ribonucleoprotein)	RNA decapping	57 (f-g)	0.78 ± 0.09	2.91 ± 0.40 *	90.18 ± 10.57 *	3.74 ± 0.51 *	115.96 ± 21.71 *	30.97 ± 4.88 *
Lsm6 (U6 snRNA-associated Lsm protein)	RNA decapping	9 (b)	0.97 ± 0.13	0.99 ± 0.09	27.36 ± 2.41 *	1.02 ± 0.20	28.12 ± 3.65 *	27.63 ± 2.99 *
Brt1 (endoribonuclease L-PSP)	RNA decapping	15 (c)	0.69 ± 0.07	2.50 ± 0.22 *	3.49 ± 0.52 *	3.62 ± 0.48 *	5.05 ± 0.77 *	1.39 ± 0.60
Endonuclease exonuclease phosphatase family protein	RNA decapping	65 (f-g)	2.69 ± 0.31 *	4.26 ± 0.55 *	5.49 ± 0.74 *	1.59 ± 0.23	2.05 ± 0.11 *	1.29 ± 0.28
scf3 (RNA-binding protein)	Release after RNA decapping	60 (f-g)	0.53 ± 0.05 *	1.38 ± 0.16	3.37 ± 0.42 *	2.60 ± 0.35 *	6.33 ± 0.81 *	2.43 ± 0.44 *
Scp160 (RNA binding effector protein)		139 (j)	0.61 ± 0.07	0.74 ± 0.05	2.07 ± 0.15 *	1.22 ± 0.10	3.42 ± 0.29 *	2.81 ± 0.30 *
RNAPII degradation factor Def	RNAPII degradation	96 (i)	1.33 ± 0.21	4.28 ± 0.63 *	34.57 ± 4.46 *	3.21 ± 0.45 *	25.97 ± 3.07 *	8.08 ± 1.01 *
RNA helicase DBP2	mRNA decay	60 (f-g)	0.75 ± 0.09	1.09 ± 0.13	6.02 ± 0.72 *	1.45 ± 0.22	7.99 ± 0.98 *	5.50 ± 0.70 *
Cerato-platanin (FGSG_04471)	Foam	24 (d)	1.28 ± 0.17	6.03 ± 0.84 *	13.93 ± 1.21 *	4.72 ± 0.43 *	10.89 ± 1.07 *	2.31 ± 0.19 *
nsp1 (nucleoporin)	Gel, mRNA transport	70 (h)	0.54 ± 0.08 *	1.24 ± 0.26	> 2 *	2.32 ± 0.33 *	> 2 *	> 2 *

\* indicates a statistically significant difference ( $p < 0.05$ ) between the two samples, **Ratio > 2 (bold)** or **Ratio < 0.5 (bold italic)** (+/- 10 %): difference of level between the two samples.

Boxes containing the value > 2 indicate that the divisor value of the ratio was 0 (compound not detected in the sample).

culture filtrates as secretion products of filamentous fungi (Boddi et al., 2004) as well as cell wall constituents of fungal hyphae and spores (González-Fernández et al., 2014). The results obtained suggested that the damage to fungal cells following the RNA-reduction process (Ward, 1996) induced the release of this protein from cell walls and its concentration in centrifugation supernatants (RNA-broth supernatant and centrate). Cerato-platanins are known for their self-assembling properties, with CPPs from *Trichoderma* fungi reported to form dimers (Vargas, Djonovic, Sukno, & Kenerley, 2008) and the *Trichoderma atroviride* cerato-platanin EPL1 shown to produce ordered layers at the air/water interface (Frischmann et al., 2013). The molecular weights associated with bands [d] (circa 25 kDa) and [e] (circa 50 kDa) on the SDS-PAGE gel (Fig. 1) correspond to the monomeric (24 kDa) and dimeric (48 kDa) forms of this cerato-platanin, however the composition of these two bands would need to be confirmed by sequencing. It is important to note that these results were obtained at the mid-point of the fermentation process, and further studies are needed to ascertain if these CPP profiles are also observed at other stages of fermentation.

A number of decapping proteins and nucleases involved in the mRNA decay pathway, which takes place in stress granules and processing bodies, were reported at significantly higher concentrations following the two heating steps ( $p < 0.05$ ) (Table 1). These stress-responsive proteins and enzymes are activated in response to change in the environment (such as the two heating steps of the Quorn fermentation process) and initiate the inhibition of RNA translation to reduce protein synthesis and conserve anabolic energy (Holcik & Sonenberg, 2005).

The concentration of the nucleoporin NSP1 also proved statistically higher following the RNA-reduction step ( $p < 0.05$ ). NSP1 is a component of the nuclear pore complex, which regulates the flow of molecules across the cell nuclear envelope, including the transport of mRNA from the nucleus to the cytoplasm (Marfori et al., 2011). The molecular weight of NSP1 (70 kDa) corresponds to band [h] on the SDS-PAGE gel, which displayed higher band intensity for the RNA-broth and RNA-broth deposit (Fig. 1).

Table 2 lists the major metabolites present at different concentrations in broth, RNA-broth, RNA-broth supernatant and centrate streams and previously reported as functional molecules. Several sugar alcohols, known to increase solution viscosity (Zhu, Ma, & Zhou, 2010), were present in statistically higher concentrations in RNA-broth and centrate in comparison with the broth ( $p < 0.05$ ).

Fungal cell wall components (including chitin, chitosan and glycoproteins) and cell membrane components (including sterols and sterol esters, phospholipids, lysophospholipids, glycosphingolipids and sphingomyelins) were identified in all samples. The monomer unit of chitin and chitosan (*N*-acetylglucosamine) and a derivative of this compound (*N*-acetylglucosamine-6-phosphate) were present in significantly higher concentrations in RNA-broth and centrate than in the broth ( $p < 0.05$ ). Chitin, chitosan and their derivatives, including those of fungal origin, are used by the food industry as thickening, gelling, foaming and emulsifying agents (Lapasin et al., 1996; Quintela et al., 2012). Similarly, phospholipids and lysophospholipids, which are common industry emulsifiers (Pichot, Watson, & Norton, 2013), were reported in statistically higher concentrations in the RNA-broth in comparison with the broth ( $p < 0.05$ ).

The samples contained a range of nucleotides, nucleosides and nucleobases (including a number of guanine-based compounds) and their derivatives (Table 2). The concentrations of nucleobases (including guanine) and nucleobase derivatives proved higher following the RNA-reducing step, with significantly higher levels in the RNA-broth, RNA-broth supernatant and centrate in comparison with the broth ( $p < 0.05$ ). 8-hydroxy-2'-deoxy guanosine (a guanine-based nucleoside derivative) and guanosine 5'-diphosphate GDP (guanine-based nucleoside diphosphate) were not modified by the RNA-reduction step but their concentrations increased following the second heating step, with statistically higher levels in the centrate in comparison with the broth and RNA-broth ( $p < 0.05$ ). Guanine and guanine-based nucleosides and

nucleotides have previously been reported for their thickening and gelling properties, which result from the self-associating ability of guanine (Peters & Davis, 2016). The higher concentrations of guanine following the RNA-reducing step was due to the breakdown of cellular RNA via the mRNA decay pathway, which released nucleotides which were subsequent broken down into nucleosides and nucleobases. The higher levels of guanosine derivative and guanosine diphosphate reported after the second heating step could result from further breakdown of RNA nucleotides via the mRNA decay pathway and/or from the breakdown of DNA nucleotides at this higher temperature (90 °C).

### 3.3. Rheological properties

Unheated solutions (10 % w/w NCM) of the broth, broth deposit, RNA-broth and RNA-broth deposit (Fig. 2a and b) showed significantly higher viscoelasticity ( $p < 0.05$ ) than the WPC control (which displayed a viscosity below 0.1 Pa.s and a 0.13 Pa elastic modulus, results not shown). The RNA-broth samples (whole stream and deposit) proved more viscoelastic than their broth counterparts ( $p < 0.05$ ), and the deposits (broth and RNA-broth) proved more viscoelastic than their whole stream counterparts ( $p < 0.05$ ) (Fig. 2a and b). The power-law model results confirmed that the RNA-broth deposit was the most viscous sample (with the highest K value of 165.62 Pa.s), followed by the RNA-broth (75.23 Pa.s), broth deposit (24.55 Pa.s) and broth (9.36 Pa.s). The model results also highlighted that the RNA-broth deposit displayed the highest rate of shear-thinning (with the lowest  $n-1$  value of  $-1.31$ ), followed by the RNA-broth ( $-0.99$ ), broth deposit ( $-0.82$ ) and broth ( $-0.64$ ). The  $R^2$  values obtained for the different samples ranged from 0.98 to 0.99.

The concentration of fungal filaments in the broth and RNA-broth samples (Fig. 2a) contributed to their high viscosity. A preliminary screening study showed that the rheological properties of the fermentation streams depended on the concentration of fungal filaments throughout the cycle (results not shown). Similarly, a high concentration of *Aspergillus terreus* filamentous pellets in fermentation broths was previously reported to correlate with an increase in viscosity (Porcel, Casas Lopez, Sanchez Perez, Fernandez Sevilla, & Chisti, 2005).

These results also confirmed our previous findings (Lonchamp et al., 2019) that the large hyphal aggregates present in the functional centrate extract (R100) were associated with its high viscoelasticity. The higher viscoelasticity of RNA-broth and RNA-broth deposit solutions in comparison with broth and broth deposit samples could then be due to their higher concentration of entangled fungal filaments, as observed on confocal micrographs (Fig. 2b). The impact of temperature on hyphal aggregation was previously demonstrated by Nyman et al. (2013) for the filamentous fungus *Rhizopus sp.*, which suggests that the RNA-reducing step enhanced the interpenetration of filaments.

The broth, broth deposit, RNA-broth and RNA-broth deposit all displayed a gel-like behaviour, which resulted from the entanglement of the fungal filaments as previously reported for mycoprotein hyphae (Finnigan, 2011). This entanglement process results from combined hydrophobic and electrostatic interactions between surface constituents of the filaments, including proteins or polysaccharides (Zhang & Zhang, 2016). The gels obtained with the broth, broth deposit, RNA-broth and RNA-broth deposit proved significantly more viscoelastic ( $p < 0.05$ ) than WPC gels (which displayed a final elasticity of 1,364 Pa, results not shown). Similarly to their unheated solutions, the RNA-broth gels (whole stream and deposit) proved more viscoelastic than their broth counterparts ( $p < 0.05$ ), whilst gels prepared with the deposits (broth and RNA-broth) proved more viscoelastic than ones prepared with their whole stream counterparts ( $p < 0.05$ ) (Fig. 2a and b), which was due to different concentrations of fungal filaments.

In addition to the contribution of the fungal material, a number of compounds with previously reported thickening and/or gelling properties were present in the broth and RNA-broth samples and contributed to their high viscosity and gelling properties, including the nucleoporin

**Table 2**  
Metabolomic comparison of the fermentation broth, RNA-broth, RNA-broth centrifugation supernatant and centrate.

Group	Subgroup	Reported functional properties	Centrate/RNA-broth supernatant		Centrate/RNA-broth		Centrate/Broth		RNA-broth supernatant/RNA-broth		RNA-broth supernatant/Broth		RNA-broth/Broth	
			pos	neg	pos	neg	pos	neg	pos	neg	pos	neg	pos	neg
Glycosyldiglycerides (Glycosyl-DG)	Monogalactosyl-DG	F, E	0.82± 0.11	0.86± 0.10	1.60± 0.19	1.76± 0.22	1.25± 0.09	1.79± 0.18	1.94* ± 0.26	2.05* ± 0.22	1.52± 0.67	2.09* ±	0.78± 0.09	1.02 ± 0.12
	Digalactosyl-DG		n/a	<b>0.01*</b> ± <b>0.01</b>	n/a	<b>0.01*</b> ± <b>0.01</b>	n/a	1.00± 0.15	n/a	1.81± 0.23	n/a	> 2*	n/a	> 2*
Phospholipids	Phosphatidyl-ethanolamines	E	1.50± 0.23	<b>4.38*</b> ± <b>0.48</b>	<b>0.16*</b> ± <b>0.03</b>	0.75± 0.09	0.78± 0.08	1.86± 0.21	<b>0.11*</b> ± <b>0.02</b>	<b>0.17*</b> ± <b>0.02</b>	<b>0.52*</b> ± <b>0.04</b>	<b>0.42*</b> ±	<b>4.81*</b> ±	<b>2.47*</b> ±
Lysophospholipids	Lysophosphatidyl-inositols	E	0.83± 0.10	<b>0.52*</b> ± <b>0.04</b>	0.96± 0.11	<b>0.26*</b> ± <b>0.04</b>	<b>2.17*</b> ± <b>0.19</b>	<b>2.41*</b> ±	1.16± 0.03	<b>0.50*</b> ± <b>0.04</b>	<b>2.62*</b> ± <b>0.28</b>	<b>4.59*</b> ±	<b>2.26*</b> ±	<b>9.13*</b> ±
	Lysophosphatidyl-Serines	E	<b>0.49*</b> ± <b>0.06</b>	<b>2.24*</b> ± <b>0.30</b>	<b>0.02*</b> ± <b>0.01</b>	1.42± 0.18	> 2*	<b>116.87*</b> ±	<b>0.04*</b> ± <b>0.01</b>	0.63± 0.06	> 2*	<b>52.09*</b> ± <b>4.64</b>	> 2*	<b>82.58*</b> ± 8.92
Sugar alcohols		V	1.12± 0.09	1.71± 0.21	1.06± 0.11	1.23± 0.16	<b>9.24*</b> ± <b>0.85</b>	<b>2.72*</b> ±	0.95± 0.12	0.72± 0.08	<b>8.28*</b> ± <b>0.94</b>	1.60± 0.23	<b>8.68*</b> ±	<b>2.22*</b> ± 0.39
Polysaccharides	Chitin (monomer)	F, E, V, G	1.25± 0.04	n/a	<b>0.52*</b> ± <b>0.08</b>	n/a	> 2*	n/a	<b>0.41*</b> ± <b>0.06</b>	n/a	> 2*	n/a	> 2*	n/a
	Chitin phosphate	F, E, V, G	n/a	1.23± 0.31	n/a	0.78± 0.98	n/a	<b>8.95*</b> ±	n/a	0.63± 0.08	n/a	<b>7.28*</b> ±	n/a	<b>11.53*</b> ± 1.42
	Inulin	V, G	1.10± 0.18	n/a	1.15± 0.14	n/a	0.99± 0.12	n/a	1.05± 0.11	n/a	0.90± 0.09	n/a	0.86± 0.07	n/a
	Galactan	V, G	1.08± 0.15	> 2*	0.80± 0.09	> 2*	1.05± 0.18	1.65± 0.13	0.74± 0.07	<b>0.01*</b> ± <b>0.01</b>	0.97± 0.11	1.00± 0.14	1.31± 0.14	> 2*
Nucleobases	Nucleobases	V, G	<b>0.01*</b> ± <b>0.01</b>	<b>0.44*</b> ± <b>0.03</b>	<b>0.01*</b> ± <b>0.01</b>	<b>0.34*</b> ± <b>0.05</b>	1.00± 0.09	<b>3.74*</b> ±	1.31± 0.38	0.77± 0.09	> 2*	<b>8.44*</b> ±	> 2*	<b>10.92*</b> ± 1.39
	Derivatives	V, G	0.79± 0.09	0.62± 0.11	0.82± 0.05	0.10	<b>1.99*</b> ± <b>0.14</b>	<b>3.25*</b> ±	0.78± 0.06	0.94± 0.12	<b>2.51*</b> ± <b>0.31</b>	<b>3.73*</b> ±	<b>3.23*</b> ±	<b>3.99*</b> ± 0.48
	Guanine	V, G	n/a	<b>0.44*</b> ± <b>0.03</b>	n/a	<b>0.34*</b> ± <b>0.05</b>	n/a	<b>3.74*</b> ±	n/a	0.77± 0.09	n/a	<b>8.44*</b> ±	n/a	<b>10.92*</b> ± 01.39
Nucleosides	Deoxyribonucleoside	V, G	<b>0.52*</b> ± <b>0.07</b>	<b>0.52*</b> ± <b>0.04</b>	0.58± 0.06	1.49± 0.18	0.68± 0.04	<b>2.28*</b> ±	1.12± 0.18	<b>2.87*</b> ± <b>0.29</b>	1.30± 0.14	<b>4.40*</b> ±	1.17± 0.23	1.53± 0.18
	Ribonucleoside derivatives	V, G	<b>0.26*</b> ± <b>0.02</b>	<b>2.25*</b> ± <b>0.26</b>	<b>0.24*</b> ± <b>0.02</b>	> 2*	> 2*	<b>6.43*</b> ±	0.92± 0.11	> 2*	> 2*	<b>2.86*</b> ±	> 2*	<b>0.01*</b> ± 0.01
	Deoxyribonucleoside derivatives	V, G	<b>0.40*</b> ± <b>0.05</b>	n/a	<b>0.19*</b> ± <b>0.07</b>	n/a	> 2*	n/a	<b>0.49*</b> ± <b>0.06</b>	n/a	> 2*	n/a	> 2*	n/a
	8-hydroxy-2'-deoxy Guanosine	V, G	1.00± 0.07	n/a	> 2*	n/a	> 2*	n/a	> 2*	n/a	> 2*	n/a	1.00± 0.11	n/a
Ribonucleoside monophosphates		V, G	<b>2.21*</b> ± <b>0.28</b>	> 2*	<b>2.15*</b> ± <b>0.19</b>	<b>2.03*</b> ± <b>0.09</b>	> 2*	<b>2.40*</b> ±	0.97± 0.08	<b>0.01*</b> ± <b>0.01</b>	> 2*	<b>0.01*</b> ±	> 2*	1.18± 0.20
Ribonucleoside diphosphates	Total	V, G	<b>0.34*</b> ± <b>0.03</b>	<b>5.82*</b> ± <b>0.55</b>	<b>0.21*</b> ± <b>0.03</b>	<b>4.82*</b> ± <b>0.37</b>	0.87± 0.10	<b>49.06*</b> ±	0.61± 0.09	0.83± 0.09	<b>2.53*</b> ± <b>0.34</b>	<b>8.43*</b> ±	<b>4.12*</b> ±	<b>10.19*</b> ± 1.23
	Guanosine 5'-diphosphate GDP	V, G	> 2*	<b>4.32*</b> ± <b>0.40</b>	> 2*	> 2*	> 2*	> 2*	1.00± 0.08	> 2*	1.00± 0.11	> 2*	1.00± 0.07	1.00± 0.12
Nucleoside diphosphate derivatives	Ribonucleoside diphosphate glycosyl aminoacids	V, G	<b>0.01*</b> ± <b>0.01</b>	<b>3.48*</b> ± <b>0.42</b>	<b>0.01*</b> ± <b>0.01</b>	> 2*	<b>0.01*</b> ± <b>0.01</b>	<b>184.38*</b> ±	0.53± 0.07	> 2*	<b>7.38*</b> ± <b>0.83</b>	<b>52.95*</b> ±	<b>13.86*</b> ± <b>1.76</b>	<b>0.01*</b> ± 0.01
	Ribonucleoside diphosphate fatty acyl glycosides	F, E, V, G	n/a	1.72± 0.22	n/a	<b>2.63*</b> ± <b>0.40</b>	n/a	<b>20.22*</b> ±	n/a	1.53± 0.23	n/a	<b>11.78*</b> ±	n/a	<b>7.68*</b> ± 0.85

Calculations based on compounds reported in positive (pos) or negative (neg) ionisation mode, F: foam, E: emulsion, V: viscosity, G: gel.

\* indicates a statistically significant difference ( $p < 0.05$ ) between the two samples, **Ratio** > 2 (**bold**) or **Ratio** < 0.5 (**bold italic**) (+/- 10 %): difference of level between the two samples.

Boxes containing the value > 2 indicate that the divisor value of the ratio was 0 (compound not detected in the sample).

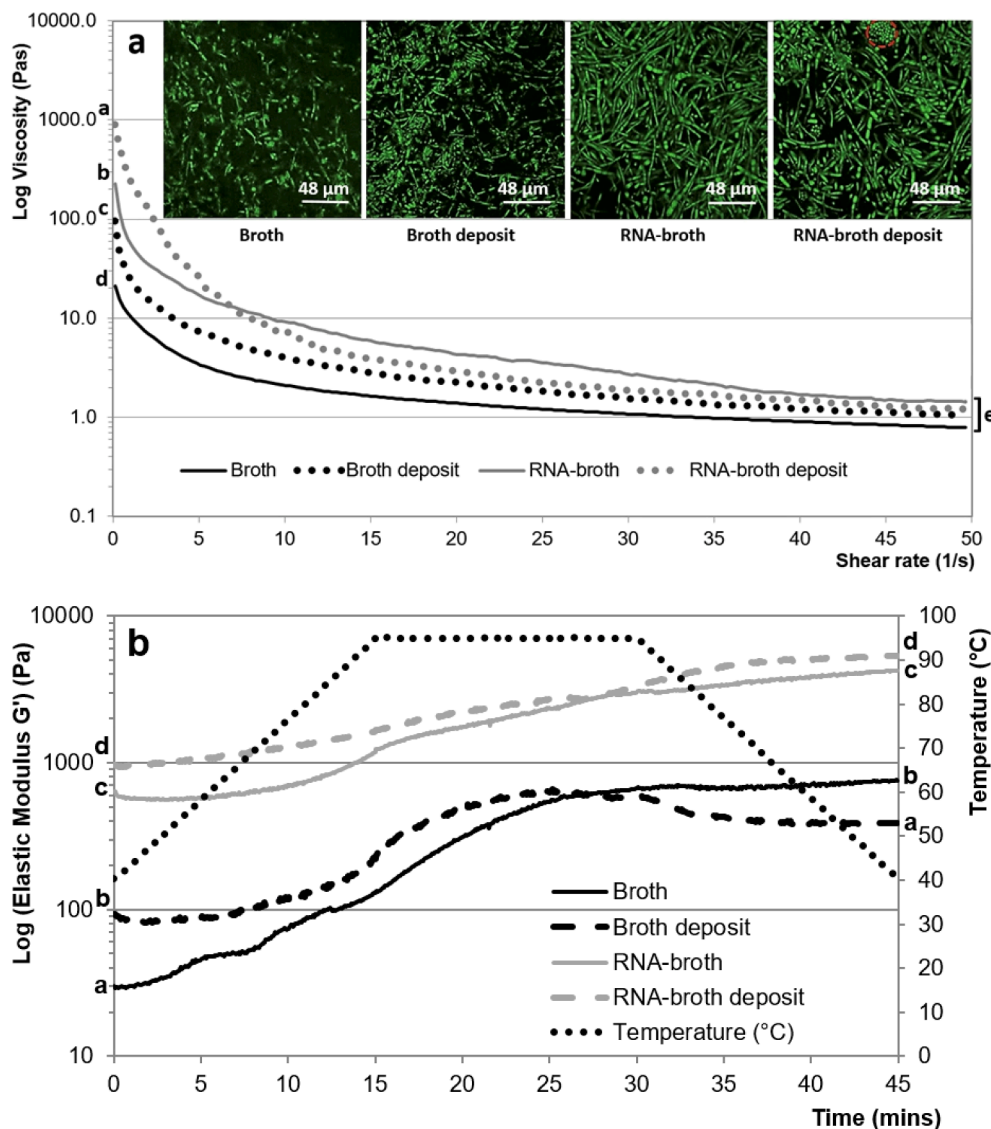


**Fig. 2.** Viscosity profiles during shear rate increase (a) and elastic modulus  $G'$  profiles during gelation (b) of the broth, RNA-broth and their centrifugation deposits (10 % w/w NCM concentration,  $n = 3$ ) with corresponding confocal micrographs of the solutions (Rhodamine B dye, magnification  $\times 10$ ). Different letters indicate statistically significant differences ( $p < 0.05$ ) in either viscosity (at either the pre- or post-shear state) or elastic modulus (at either the pre- or post-gelation state).

NSP1 (Ader et al., 2010), chitin and chitosan (Lapasin et al., 1996), inulin (Kurakake et al., 2008), galactan (Delattre, Fenoradosoa, & Michaud, 2011) and guanine and guanine-based nucleosides and nucleotides (Peters & Davis, 2016) (Table 2).

In particular, chitin and chitosan were reported at statistically higher levels in the RNA-broth in comparison with the broth ( $p < 0.05$ ) and were further concentrated in the deposits due to their insolubility in water (confirmed by their significantly lower concentrations ( $p < 0.05$ ) in RNA-broth supernatant in comparison with the RNA-broth in Table 2). These differences contributed to the higher rheological properties of the RNA-broth deposit. Similarly, the release of guanine following the RNA-reducing step and its concentration in the RNA-broth deposit due to its relative insolubility in water (confirmed by its statistically lower concentration ( $p < 0.05$ ) in the RNA-broth supernatant than in the RNA-broth in Table 2) contributed to the higher viscoelasticity of the RNA-broth deposit solution and its resulting gel. Finally, the significantly higher concentrations ( $p < 0.05$ ) of the nucleoporin NSP1 in the RNA-broth and RNA-broth supernatant in comparison with the broth (Table 1) contributed to the higher viscoelasticity of the RNA-broth gel in comparison with the broth gel. NSP1 is a constituent of the permeability barrier of the nuclear pore protein complex, which

hydrogel structure results from the cross-linking of phenylalanine/glycine-rich (FG) domains of the nucleoporins (Ader et al., 2010). Furthermore, artificially-engineered proteins designed using the functional sequence of NSP1 produced strong hydrogels (Kim et al., 2015).

#### 3.4. Foaming properties

All the samples displayed higher foaming abilities than the WPC control, except for the RNA-broth (Fig. 3a and 3b). The standard deviations calculated for the different data points ranged from 0.3 to 0.1 cm (not shown on Fig. 3 to maintain clarity). The high foaming ability of the centrate confirms the observation that it foams in the centrifuge during the Quorn process. The foams produced with all nine mycoprotein samples proved more stable (between 340 min and at least 380 min) than the WPC foams (320 min). The foams prepared with broth, RNA-broth, RNA-broth supernatant and centrate supernatant displayed the highest stabilities (at least 380 min).

The low foaming ability but high foam stability reported for the RNA-broth could be due to its high entanglement of fungal filaments following the RNA-reduction step and the resulting high viscosity. We previously reported a similar foaming profile for the functional centrate

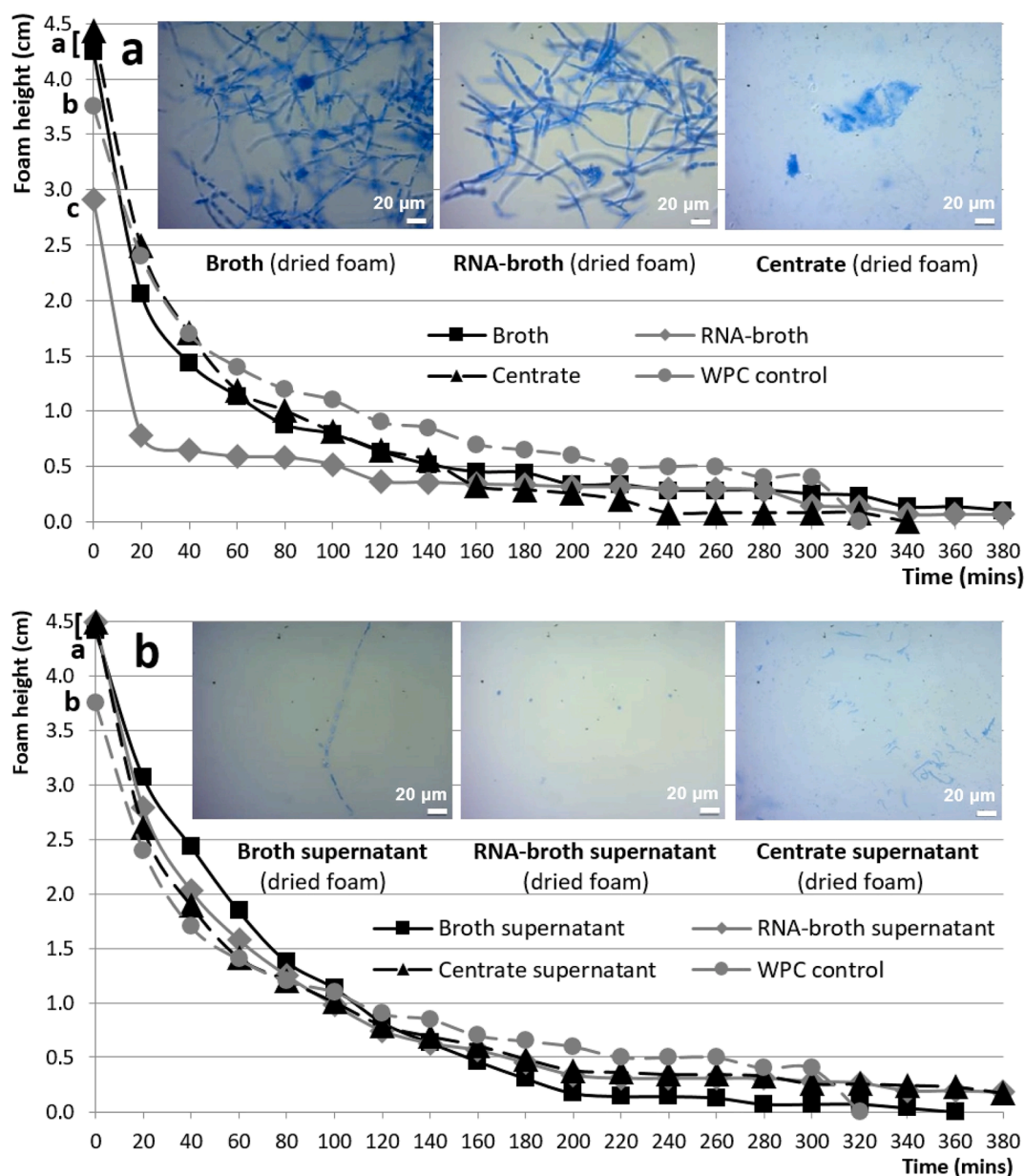


**Fig. 3.** Foaming ability and foam stability profiles of the broth, RNA-broth and centrate (a) and their centrifugation supernatants (b) (1 % w/w NCM concentration,  $n = 6$ ) with corresponding bright-field micrographs of the resulting dried foams (1 % w/w NCM concentration, magnification  $\times 50$ ). Different letters indicate statistically significant differences ( $p < 0.05$ ) in foaming ability (initial data point).

extract (R100), which was characterised by a high concentration of large hyphal aggregates (Lonchamp et al., 2019). A dense network of hyphal material trapping air bubbles was observed in R100 foams, which only allowed a small number of air bubbles to form and was in agreement with the low foaming ability measured for R100. This filamentous network also reduced the likelihood of foam breakdown by drainage and coalescence because of high viscosity. Such mechanism was also described for the filamentous fungus *Aspergillus terreus*, which highly viscous fermentation media displayed low gas – liquid mass transfer (Porcel et al., 2005). The high viscosity reported for RNA-broth solutions thus only allowed a small number of air bubbles to form, which accounted for the poor foaming ability, but at the same time stabilised these few air bubbles by limiting their movement, which explained the high foam stability.

The high stability reported for broth and RNA-broth foams could then result from the concentration of fungal filaments in these samples, while the presence of foam-positive molecules in the RNA-broth and

centrate supernatants (Table 2) contributed to their high foaming ability and stability. In particular the concentrations of the cerato-platanin protein in the RNA-broth and centrate supernatant foams proved significantly higher ( $p < 0.05$ ) than in the other samples (Table 1), contributing to the high stabilities of their foams. Frischmann et al. (2013) previously reported high foaming properties for cerato-platanin EPL1 solutions from *Trichoderma atroviride*. In addition, the cell wall components chitin and chitosan, which foaming properties were previously reported (Lapasin et al., 1996), were also present in statistically higher concentrations following the RNA-reducing step ( $p < 0.05$ ) and contributed to the foaming properties of the RNA-broth and centrate samples.

Moreover, the presence of *Fusarium venenatum* cells and/or spores in the samples could also have stabilised the foams as bacterial cells and spores fall within the range of shapes and sizes suitable for Pickering stabilisation of foams and emulsions (Lam et al., 2014).

### 3.5. Emulsifying properties

Emulsions prepared with the three supernatant samples (broth, RNA-broth and centrate), broth and broth deposit displayed similar or statistically higher emulsifying activity index (EAI) than WPC emulsions ( $p < 0.05$ ) and statistically higher EAI values than emulsions prepared with the other samples ( $p < 0.05$ ) (Fig. 4a). The emulsifying stability index (ESI) obtained for broth, broth supernatant and RNA-broth deposit emulsions also proved similar or significantly higher than WPC emulsions ( $p < 0.05$ ) and significantly higher than emulsions prepared with the other samples ( $p < 0.05$ ) (Fig. 4a). The emulsions prepared with all the samples displayed similar or statistically smaller mean oil droplet sizes (D[3,2], surface weighted mean values) than WPC emulsions ( $p < 0.05$ ), except for centrate deposit emulsions (Fig. 4b). Emulsions prepared with broth, broth deposit (Fig. 4b), RNA-broth and RNA-broth deposit (Fig. 4b) exhibited a network of fungal filaments surrounding the oil droplets.

The RNA-broth deposit emulsions displayed the lowest EAI ( $p < 0.05$ , similar to centrate deposit) but the highest ESI of all samples ( $p < 0.05$ ). Similarly to the foaming results, the high entanglement of fungal filaments in the RNA-broth deposit following the RNA-reduction process and the resulting high viscosity (Fig. 2) limited the number of oil droplets that could be formed, which led to a poor EAI. However this entanglement and high viscosity also stabilised these oil droplets by separating them and limiting their movement (thus preventing coalescence of the droplets and the resulting destabilisation of the emulsion), which resulted in high ESI. Similarly, the low EAI but similar ESI of the centrate deposit in comparison with the other samples could also be

explained by the concentration of aggregated fungal material in this sample following the second heating step.

Confocal micrographs showed rings of small hyphal fragments of heterogeneous length (5–10  $\mu\text{m}$ ) around oil droplets in broth, broth deposit, RNA-broth and RNA-broth deposit emulsions (Fig. 4b). Similar rings of hyphal material were observed in our previous study (Lonchamp et al., 2020) in emulsions prepared with the sonicated centrate extract. These small hyphal fragments possibly played a role in forming and stabilising oil droplets through a Pickering-type stabilisation process, as previously reported for a range of bacterial cells and spores (Binks et al., 2005; Dorobantu et al., 2004). The results obtained suggested that the optimisation and control of the size of these hyphal fragments via optimised processing could further improve the stability of the emulsions.

A range of metabolites with known emulsifying properties, including cell wall chitin and chitosan (Lapasin et al., 1996) and cell membrane phospholipids (Pichot et al., 2013), were reported in statistically higher concentrations following the RNA-reducing heat-shock treatment ( $p < 0.05$ ) and contributed to the emulsifying properties of the RNA-broth and centrate samples. In addition, the significantly higher levels of the cerato-platanin in the RNA-broth supernatant and centrate in comparison with the other samples ( $p < 0.05$ ) contributed to the high EAI and small oil droplet sizes obtained with the RNA-broth and centrate supernatants. Pitocchi et al. (2020) previously reported highly stable emulsions prepared with cerato-platanin isolates from the marine fungi *Aspergillus terreus* MUT 271 and *Trichoderma harzianum* MUT 290.

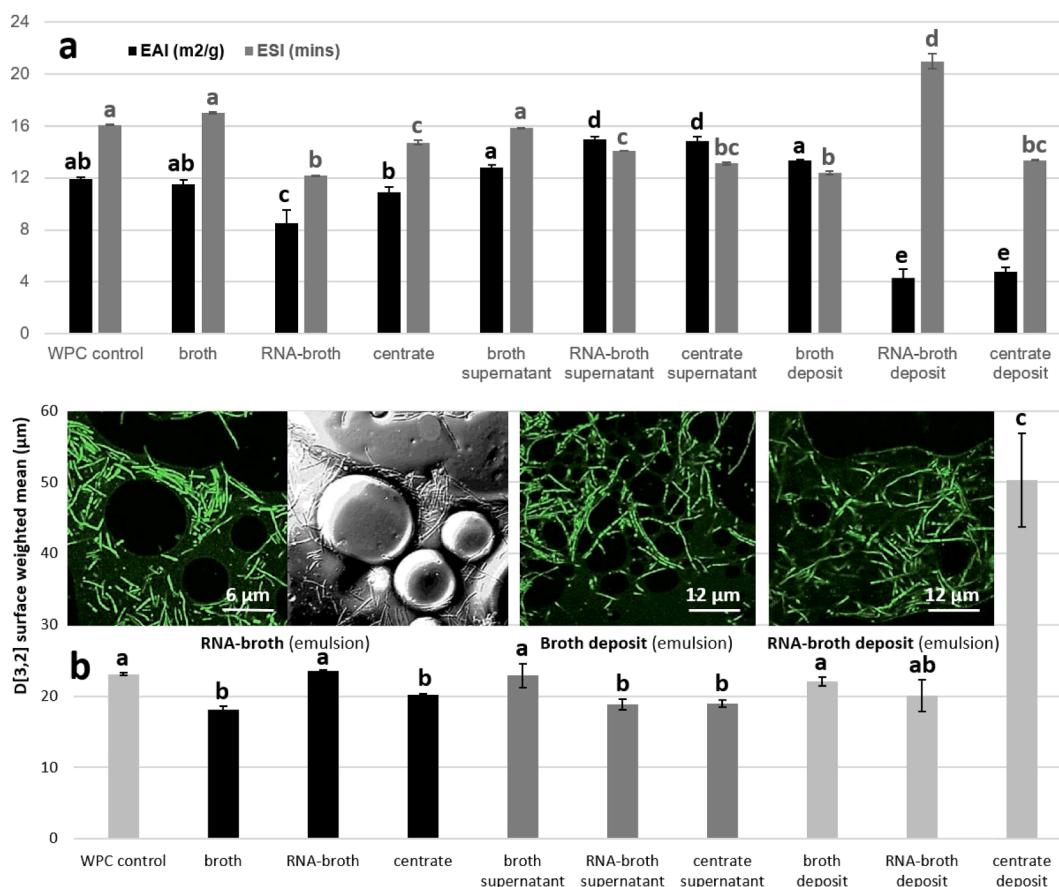


**Fig. 4.** Emulsifying ability index (EAI) and emulsifying stability index (ESI) of the fermentation broth, RNA-reduced broth and centrate whole streams, centrifugation supernatants and deposits (a) and average oil droplet size of the resulting emulsions (b) (1 % w/w NCM concentration,  $n = 4$ ) with corresponding confocal micrographs of the emulsions (Rhodamine B dye, magnification  $\times 10$  or  $\times 50$ ). Different letters indicate statistically significant differences ( $p < 0.05$ ) in either EAI, ESI or average oil droplet size.

#### 4. Conclusions

This study identified previously unreported gelling, foaming and/or emulsifying properties for the different Quorn fermentation streams, highlighting opportunities to use the Quorn process to produce novel sustainable alternatives to animal-derived functional ingredients. The broth, broth deposit, RNA-broth and RNA-broth deposit showed high potential as novel thickening and gelling agents. Solutions of these samples displayed high viscosity (with a 904.43 Pa.s viscosity reported for the RNA-broth deposit) due to their concentration of fungal filaments, whilst hydrogels prepared with these solutions proved highly viscoelastic (with a 5,320 Pa elastic modulus reported for RNA-broth deposits gels) due to the high levels of entangled fungal filaments resulting from the gelation process. The RNA-broth and centrate supernatants showed potential as novel foaming agents with high foaming stability (380 min via a frothing assay) due to their higher concentrations of foam-positive molecules following the RNA-reducing step, including the cell wall components chitin and chitosan and a cerato-platanin. The broth and broth supernatant showed potential as novel emulsifying agents with high EAI and ESI (12.80 m<sup>2</sup>/g and 15.84 mins for the broth supernatant) and low emulsion droplet sizes (18.09 µm for the broth) due to the presence of a suitable network of fungal filaments surrounding the oil droplets in the broth and of emulsion-positive molecules in the broth supernatant. In particular, due to its high yield and reduced nucleic acid content, the RNA-broth deposit is highly suitable for further processing into a novel gelling agent powder (centrifugation deposit) and foaming agent powder (centrifugation supernatant).

This study also reported the impact of the two heating steps of the Quorn fermentation process (RNA-reducing heat-shock treatment of the fermentation broth and second heating step on the RNA-reduced broth) on mycoprotein composition, structure and functionality. The RNA reduction step resulted in a higher level of entanglement of fungal filaments in the RNA-broth and RNA-broth deposit, which contributed to their high rheological properties. Following the two heating steps, a number of small spherical components were observed in the centrate and could correspond to processing bodies (p-bodies) or stress granules formed as a response to the stress caused by the heat-shock RNA-reduction process. The higher guanine concentration reported in the RNA-broth following the mRNA decay pathway, which occurs in stress granules and p-bodies, contributed to its higher rheological properties in comparison with the fermentation broth.

The results obtained confirmed the three hypotheses of the study, stating that the functionality of the broth, RNA-reduced and their deposits is mainly governed by the hyphal material whilst the functionality of the supernatants is mainly due to surface-active molecules, and that the two heating steps of the process significantly modify the functionality and structure of the mycoprotein material.

Future studies will be carried out to further characterise the contribution of the fungal structures (filament aggregates and small fragments) and of surface-active molecules (including the cerato-platanin, chitin and chitosan and guanine and guanine-based nucleosides and nucleotides) to the functionality of the different streams. Future work will investigate the optimisation of the Quorn fermentation process for the production of novel sustainable functional ingredients and their potential application in the food industry.

#### CRedit authorship contribution statement

**Julien Lonchamp:** Conceptualization, Data curation, Formal analysis, Investigation, Methodology, Validation, Writing – original draft, Writing – review & editing. **Kelly Stewart:** Formal analysis, Investigation, Methodology. **Claire D. Munialo:** Investigation, Methodology, Writing – review & editing. **Laurence Evans:** Formal analysis, Investigation. **Muyiwa Akintoye:** Conceptualization, Methodology. **Susan Gordon:** Conceptualization, Methodology. **Paul S. Clegg:** Validation,

Writing – original draft, Writing – review & editing. **Nik Willoughby:** Methodology, Validation. **Stephen R. Euston:** Conceptualization, Formal analysis, Methodology, Validation, Writing – original draft, Writing – review & editing.

#### Declaration of Competing Interest

The authors declare that they have no known competing financial interests or personal relationships that could have appeared to influence the work reported in this paper.

#### Data availability

Data will be made available on request.

#### Acknowledgements

The authors wish to thank Dr Tim Finnigan from Quorn Foods for his support during this project. This work was supported by Innovate UK (grant number TS/N001028/1 Functional mycoprotein from the Quorn fermentation process as novel sustainable ingredient).

#### References

- Ader, C., Frey, S., Maas, W., Broder Schmidt, H., Görlich, D., & Baldus, M. (2010). Amyloid-like interactions within nucleoporin FG hydrogels. *PNAS*, *107*(14), 6281–6285. <https://doi.org/10.1073/pnas.0910163107>
- Binks, B. P., Clint, J. H., Mackenzie, G., Simcock, C., & Whitby, C. P. (2005). Naturally occurring spore particles at planar fluid interfaces and in emulsions. *Langmuir*, *21* (18), 8161–8167. <https://doi.org/10.1021/la0513858>
- Boddi, S., Comparini, C., Calamassi, R., Pazzagli, L., Cappugi, G., & Scala, A. (2004). Cerato-platanin protein is located in the cell walls of ascospores, conidia and hyphae of *Ceratocystis fimbriata* f. sp. platani. *FEMS Microbiology Letters*, *233*, 341–346. <https://doi.org/10.1111/j.1574-6968.2004.tb09501.x>
- Colosimo, R., Mulet-Cabero, A. I., Warren, F. J., Edwards, C. H., Finnigan, T. J. A., & Wilde, P. J. (2020). Mycoprotein ingredient structure reduces lipolysis and binds bile salts during simulated gastrointestinal digestion. *Food & Function*, *11*(12), 10896–10906. <https://doi.org/10.1039/D0FO02002H>
- Delattre, C., Fenoradosa, T. A., & Michaud, P. (2011). Galactans: An overview of their most important sourcing and applications as natural polysaccharides. *Brazilian Archives of Biology and Technology*, *54*(6), 1075–1092. <https://doi.org/10.1590/S1516-89132011000600002>
- Denny, A., Aisbitt, B., & Lunn, J. (2008). Mycoprotein and health. *British Nutrition Bulletin*, *33*, 298–310. <https://doi.org/10.1111/j.1467-3010.2008.00730.x>
- Dorobantu, L. S., Yeung, A. K. C., Foght, J. M., & Gray, M. R. (2004). Stabilization of oil-water emulsions by hydrophobic bacteria. *Applied and Environmental Microbiology*, *70* (10), 6333–6336. <https://doi.org/10.1128/AEM.70.10.6333-6336.2004>
- Finnigan, T. (2011). Mycoprotein: Origins, production and properties. In G. O. Phillips, & P. A. Williams (Eds.), *Handbook of food proteins* (pp. 335–352). Woodhead Publishing.
- Finnigan, T., Lemon, M., Allen, B., & Patton, I. (2010). Mycoprotein life cycle analysis and the food 2030 challenge. *Aspects of Applied Biology*, *102*, 81–90.
- Frischmann, A., Neudl, S., Gaderer, R., Bonazza, K., Zach, S., Gruber, S., ... Seidl-Seiboth, V. (2013). Self-assembly at air/water interfaces and carbohydrate binding properties of the small secreted protein EPL1 from the fungus *Trichoderma atroviride*. *The Journal of Biological Chemistry*, *288*, 4278–4287. <https://doi.org/10.1074/jbc.M112.427633>
- González-Fernández, R., Aloria, K., Valero-Galván, J., Redondo, I., Arizmendi, J. M., & Jorrín-Novo, J. V. (2014). Proteomic analysis of mycelium and secretome of different *Botrytis cinerea* wild-type strains. *Journal of Proteomics*, *9*, 195–221. <https://doi.org/10.1016/j.jprot.2013.06.022>
- Griffen, A. M., Wiebe, M. G., Robson, G. D., & Trinci, A. P. J. (1997). Extracellular proteases produced by the Quorn® myco-protein fungus *Fusarium graminearum* in batch and chemostat culture. *Microbiology*, *143*(9), 3007–3013. <https://doi.org/10.1099/00221287-143-9-3007>
- Havea, P., Watkinson, P., & Kuhn-Sherlock, B. (2009). Heat-Induced Whey Protein Gels: Protein-Protein Interactions and Functional Properties. *Journal of Agricultural and Food Chemistry*, *57*, 1506–1512. <https://doi.org/10.1021/jf802559z>
- Holcik, M., & Sonenberg, N. (2005). Translational control in stress and apoptosis. *Nature Reviews Molecular Cell Biology*, *6*, 318–327. <https://doi.org/10.1038/nrm1618>
- Huang, H.-T., Maruyama, J.-I., & Kitamoto, K. (2013). *Aspergillus oryzae* AoSO is a novel component of stress granules upon heat stress in filamentous fungi. *PLoS ONE*, *8*(8), e72209.
- Kim, M., Chen, W. G., Kang, J. W., Glassman, M. J., Ribbeck, K., & Olsen, B. D. (2015). Artificially engineered protein hydrogels adapted from the nucleoporin Nsp1 for selective biomolecular transport. *Advanced Materials*, *27*(28), 4207–4212. <https://doi.org/10.1002/adma.201500752>

- Kurakake, M., Ogawa, K., Sugie, M., Takemura, A., Sugiura, K., & Komaki, T. (2008). Two types of beta-fructofuranosidases from *Aspergillus oryzae* KB. *Journal of Agricultural and Food Chemistry*, *56*, 591–596. <https://doi.org/10.1021/jf072762k>
- Lam, S., Velikov, K. P., & Velev, O. D. (2014). Pickering stabilization of foams and emulsions with particles of biological origin. *Current Opinion in Colloid & Interface Science*, *19*(5), 490–500. <https://doi.org/10.1016/j.cocis.2014.07.003>
- Lapasin, R., Stefancic, S., & Delben, F. (1996). Rheological properties of emulsions containing soluble chitosan. *Agro-food Industry High-Tech*, *7*, 12–17.
- Le Bihan, T., Martin, S. F., Chirnside, E. S., van Ooijen, G., Barrios-Llerena, M. E., O'Neill, J. S., ... Millar, A. J. (2011). Shotgun proteomic analysis of the unicellular alga *Ostreococcus tauri*. *Journal of Proteomics*, *74*, 2060–2070. <https://doi.org/10.1016/j.jprot.2011.05.028>
- Lonchamp, J., Akintoye, M., Clegg, P., & Euston, S. R. (2020). Sonicated extracts from the Quorn fermentation co-product as oil-lowering emulsifiers and high-foaming agents. *European Food Research and Technology*, *246*(4), 767–780. <https://doi.org/10.1007/s00217-020-03443-w>
- Lonchamp, J., Clegg, P. S., & Euston, S. R. (2019). Foaming, emulsifying and rheological properties of extracts from a co-product of the Quorn fermentation process. *European Food Research and Technology*, *245*(9), 1825–1839. <https://doi.org/10.1007/s00217-019-03287-z>
- Lynch, J. M., Barbano, D. M., & Fleming, J. R. (1998). Indirect and direct determination of the casein content of milk by Kjeldahl nitrogen analysis: Collaborative study. *Journal of AOAC International*, *81*, 763–774. <https://doi.org/10.1093/jaoac/81.4.763>
- Marfori, M., Mynott, A., Ellis, J. J., Mehdi, A. M., Saunders, N. F. W., Curmi, P. M., ... Kobe, B. (2011). Molecular basis for specificity of nuclear import and prediction of nuclear localization. *Biochimica et Biophysica Acta (BBA) - Molecular Cell Research*, *1813*(9), 1562–1577. <https://doi.org/10.1016/j.bbamcr.2010.10.013>
- Martin, S., Munagapati, V. S., Salvo-Chirnside, E., Kerr, L., & Le Bihan, T. (2012). Proteome turnover in the green alga *Ostreococcus tauri* by time course 15 N metabolic labeling mass spectrometry. *Journal of Proteome Research*, *11*, 476–486. <https://doi.org/10.1021/pr2009302>
- McMichael, J., Powles, C., & Butler, R. (2007). Food, livestock production, energy, climate change, and health. *Lancet*, *370*, 1253–1263. [https://doi.org/10.1016/S0140-6736\(07\)61256-2](https://doi.org/10.1016/S0140-6736(07)61256-2)
- Nyman, J., Lacintra, M. J., Westman, J. O., Berglin, M., Lundin, M., Lennartsson, P. R., & Taherzadeh, M. J. (2013). Pellet formation of zygomycetes and immobilization of yeast. *New Biotechnology*, *30*(5), 516–522. <https://doi.org/10.1016/j.nbt.2013.05.007>
- Ogunwolu, S. O., Henshaw, F. O., Mock, H. P., & Santos, A. (2009). Functional properties of protein concentrates and isolates produced from cashew (*Anacardium occidentale* L.) nut. *Food Chemistry*, *115*, 852–858. <https://doi.org/10.1016/j.foodchem.2009.01.011>
- Pappin, D. J., Hojrup, P., & Bleasby, A. J. (1993). Rapid identification of proteins by peptide-mass fingerprinting. *Current Biology*, *3*, 327–332. [https://doi.org/10.1016/0960-9822\(93\)90195-T](https://doi.org/10.1016/0960-9822(93)90195-T)
- Peters, G. M., & Davis, J. T. (2016). Supramolecular gels made from nucleobase, nucleoside and nucleotide analogs. *Chemical Society Reviews*, *45*, 3188–3206. <https://doi.org/10.1039/C6CS00183A>
- Pichot, R., Watson, R. L., & Norton, I. T. (2013). Phospholipids at the interface: Current trends and challenges. *International Journal of Molecular Sciences*, *14*, 11767–11794. <https://doi.org/10.3390/ijms140611767>
- Pitocchi, R., Cicatiello, P., Birolò, L., Piscitelli, A., Bovio, E., Varese, G. C., & Giardina, P. (2020). Cerato-platanins from marine fungi as effective protein biosurfactants and bioemulsifiers. *International Journal of Molecular Sciences*, *21*(8), 2913. <https://doi.org/10.3390/ijms21082913>
- Porcel, E. M. R., Casas Lopez, J. L., Sanchez Perez, J. A., Fernandez Sevilla, J. M., & Chisti, Y. (2005). Effects of pellet morphology on broth rheology in fermentations of *Aspergillus terreus*. *Biochemical Engineering Journal*, *26*, 139–144. <https://doi.org/10.1016/j.bej.2005.04.011>
- Quintela, S., Villarán, M. C., López De Armentia, I., & Elejalde, E. (2012). Ochratoxin a removal from red wine by several oenological fining agents: Bentonite, egg albumin, allergen-free adsorbents, chitin and chitosan. *Food Additives & Contaminants: Part A*, *29*(7), 1168–1174. <https://doi.org/10.1080/19440049.2012.682166>
- Shaw, C. D., Lonchamp, J., Downing, T., Imamura, H., Freeman, T. M., Cotton, J. A., ... Carter, K. C. (2016). In vitro selection of miltefosine resistance in promastigotes of *Leishmania donovani* from Nepal: Genomic and metabolomic characterization. *Molecular Microbiology*, *99*(6), 1134–1148. <https://doi.org/10.1111/mmi.13291>
- Vargas, W. A., Djonovic, S., Sukno, S. A., & Kenerley, C. M. (2008). Dimerization controls the activity of fungal elicitors that trigger systemic resistance in plants. *The Journal of Biological Chemistry*, *283*, 19804–19815. <https://doi.org/10.1074/jbc.M802724200>
- Ward, P. N. (1996). A process for the reduction of nucleic acid content for a fungus imperfectus. *WO Patent*, *95/23843*.
- Zhang, J., & Zhang, J. (2016). The filamentous fungal pellet and forces driving its formation. *Critical Reviews in Biotechnology*, *36*(6), 1066–1077. <https://doi.org/10.3109/07388551.2015.1084262>
- Zhu, C., Ma, Y., & Zhou, C. (2010). Densities and viscosities of sugar alcohol aqueous solutions. *Journal of Chemical & Engineering Data*, *55*(9), 3882–3885. <https://doi.org/10.1021/je9010486>